Journal of Molecular Structure 1063 (2014) 16–29

Contents lists available at ScienceDirect

Journal of Molecular Structure

journal homepage: www.elsevier.com/locate/molstruc

Quantum mechanical and spectroscopic (FT-IR, FT-Raman, ^{1}H NMR and UV) investigations of 5-nitro-2-phenylbenzoxazole

J.B. Bhagyasree [a], Hema Tresa Varghese [b], C. Yohannan Panicker [c,*], Jadu Samuel [a], Christian Van Alsenoy [d], Tugba Ertan-Bolelli [e], Ilkay Yildiz [e]

[a] Department of Chemistry, Mar Ivanios College, Nalanchira, Trivandrum, Kerala, India
[b] Department of Physics, Fatima Mata National College, Kollam, Kerala, India
[c] Department of Physics, TKM College of Arts and Science, Kollam, Kerala, India
[d] Department of Chemistry, University of Antwerp, B2610 Antwerp, Belgium
[e] Faculty of Pharmacy, Department of Pharmaceutical Chemistry, Ankara University, Tandogan, 06100 Ankara, Turkey

HIGHLIGHTS

- IR, Raman spectra and NBO analysis of 5-nitro-2-phenylbenzoxazole were reported.
- The wavenumbers are calculated theoretically using Gaussian09 software.
- The wavenumbers are assigned using PED analysis.
- The optimized geometrical parameters of 5-nitro-2-phenylbenzoxazole are in agreement with that of similar compounds.

GRAPHICAL ABSTRACT

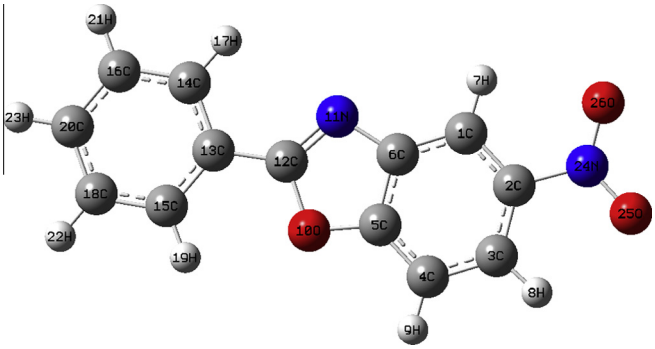

ARTICLE INFO

Article history:
Received 1 November 2013
Received in revised form 12 December 2013
Accepted 13 January 2014
Available online 21 January 2014

Keywords:
FT-IR
FT-Raman
Benzoxazole
Hyperpolarizability
PED
Antimicrobial

ABSTRACT

The optimized molecular structure, vibrational wavenumbers, corresponding vibrational assignments of 5-nitro-2-phenylbenzoxazole have been investigated experimentally and theoretically. The energy and oscillator strength calculated by Time Dependent Density Functional Theory results almost compliments with experimental findings. Gauge-including atomic orbital ^{1}H-NMR chemical shifts calculations were carried out and compared with experimental data. The HOMO and LUMO analysis is used to determine the charge transfer with in the molecule. The stability of the molecule arising from hyper-conjugative interaction and charge delocalization has been analyzed using NBO analysis. molecular electrostatic potential was performed by the DFT method and the infrared intensities and Raman activities are also been reported. Fist hyperpolarizability is calculated in order to find its role in nonlinear optics. Antimicrobial properties indicated that the title compound possessed a broad spectrum activity against the tested Gram-positive, Gram-negative bacteria.

1. Introduction

Benz-fused azoles are five-member ring compound containing both nitrogen and oxygen fused to a benzene ring. Benzoxazole does not have a weak N—O bond and contains a resonance-stabilized benzene ring and hence it is more stable and is expected to start decomposing at a temperature higher than those of its two benzisoxazole isomers under the same conditions and are a common heterocyclic scaffold in biologically active and medicinally significant compounds. The benzoxazole ring system occurs

* Corresponding author. Tel.: +91 9895370968.
E-mail address: cyphyp@rediffmail.com (C.Y. Panicker).

http://dx.doi.org/10.1016/j.molstruc.2014.01.018
0022-2860/

occasionally in nature [1,2] and benzoxazole derivatives have achieved importance in pharmacology as antibacterial or antifungal agents [3–6], HIV-1 reverse transcriptase inhibitors [7,8], topoisomerase I inhibitors [9], and antitumor agents [9–12]. Yalcin et al. [13–16] reported the synthesis and microbiological activity of 5-substituted-2-(p-substitutedphenyl)benzoxazole derivatives. Anto et al. [17] reported the vibrational spectroscopic and ab initio calculations of 5-methyl-2-(p-fluorophenyl) benzoxazole. Vibrational spectroscopic studies and ab initio calculations of 5-methyl-2-(p-methylaminophenyl)benzoxazole is reported by Ambujakshan et al. [18]. Ab initio quantum mechanical method is at present widely used for simulating IR spectrum. Such simulations are indispensable tools to perform normal coordinate analysis so that modern vibrational spectroscopy is unimaginable without involving them and time-dependent DFT (TD-DFT) calculations have also been used for analysis of the electronic spectrum and spectroscopic properties. The energies, degrees of hybridization, populations of the lone electron pairs of oxygen, energies of their interaction with the anti-bonding π^* orbitals of the benzene ring and electron density (ED) distributions and E(2) energies have been calculated by NBO analysis using DFT method to give clear evidence of stabilization originating from the hyper conjugation of various intra-molecular interactions. In the present work, IR, Raman spectra, ^{1}H NMR parameters and UV–Vis spectrum of 5-nitro-2-phenylbenzoxazole were described both experimentally and theoretically. The HOMO and LUMO analysis have been used to elucidate information regarding charge transfer within the molecule. There has been growing interest in using organic materials for nonlinear optical devices, functioning as second harmonic generators, frequency converters, electro-optical modulators, etc. because of the large second order electric susceptibilities of organic materials. Since the second order electric susceptibility is related to first hyperpolarizability, the search for organic chromophores with large first hyperpolarizability is fully justified. The organic compound showing high hyperpolarizability are those containing an electron donating group or an electron withdrawing group interacting through a system of conjugated double bonds. In this case, the electron withdrawing group NO_2 is present in the title compound.

2. Experimental details

For the synthesis of the benzoxazole derivative, using aqueous mineral acids as the condensation reagent did not provide successful results, because of the oxazole ring which was easily hydrolyzed under these conditions [19]. The title compound 5-nitro-2-phenylbenzoxazole was prepared by heating 0.01 mol 2-amino-4-nitrophenol, 0.01 mol benzoic acid in 24 g poly-phosphoric acid (PPA) and stirring for 4 h (Scheme 1). At the end of the reaction period, the residues were poured into an ice-water mixture and neutralized with excess of 10% NaOH solution extracted with ethyl acetate. Then, this solution was dried over anhydrous sodium sulfate and evaporated under diminished pressure. The residue was boiled with 200 mg charcoal in ethanol and filtered. After the evaporation of solvent in vacuo, the crude product was obtained and re-crystallized from ethanol.

The FT-IR spectrum (Fig. 1) was recorded using KBr pellets on a DR/Jasco FT-IR 6300 spectrometer. The FT-Raman spectrum (Fig. 2) was obtained on a Bruker RFS 100/s, Germany. For excitation of the

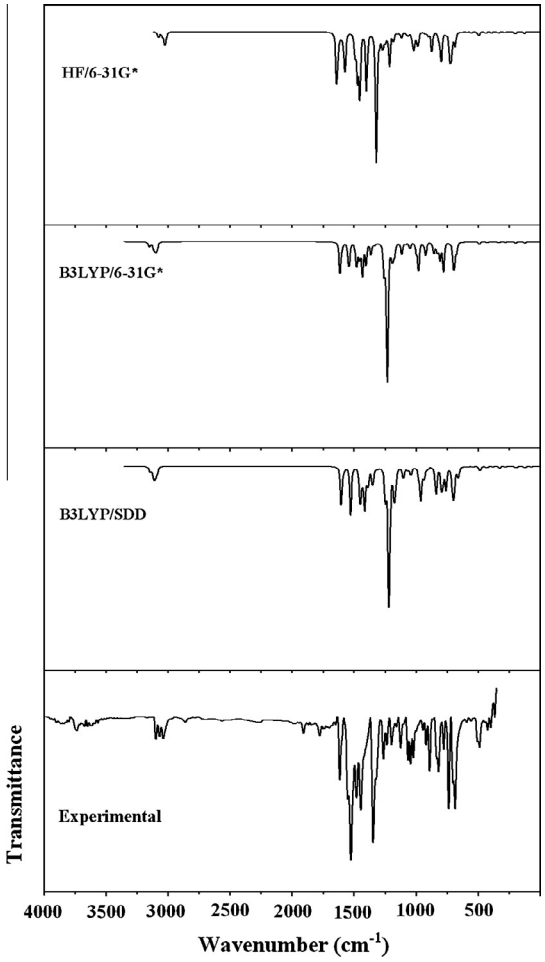

Fig. 1. FT-IR spectrum of 5-nitro-2-phenylbenzoxazole.

spectrum the emission of Nd:YAG laser was used, excitation wavelength 1064 nm, maximal power 150 mW, measurement on solid sample.

Chemical Formula: $C_{13}H_8N_2O_3$; Molecular Weight: 240.21; *m*/*z*: 240.05 (100.0%), 241.06 (14.3%), 242.06 (1.6%); Elemental Analysis: Calc./Found: C 65.00, 65.05; H 3.36, 3.40; N 11.66, 11.62; O 19.98, 19.95. ^{1}H-NMR spectrum was recorded at 400 MHz on a Varian Inova-400 spectrometer and chemical shifts were reported relative to internal TMS.

3. Computational details

Calculations of the title compound are carried out with Gaussian09 program [20] using the HF/6-31G*, B3LYP/6-31G* and Stuttagart/Dresden effective core potential (SDD) basis sets to predict the molecular structure and vibrational wavenumbers. Molecular geometry was fully optimized by Berny's optimization algorithm using redundant internal coordinates. Harmonic vibrational wavenumbers are calculated using the analytic second derivatives to confirm the convergence to minima on the potential surface. The wavenumber values computed at the Hartree–Fock level contain

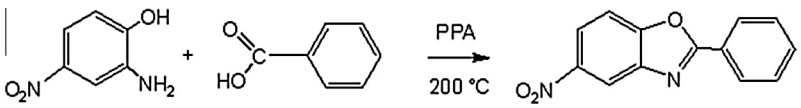

Scheme 1.

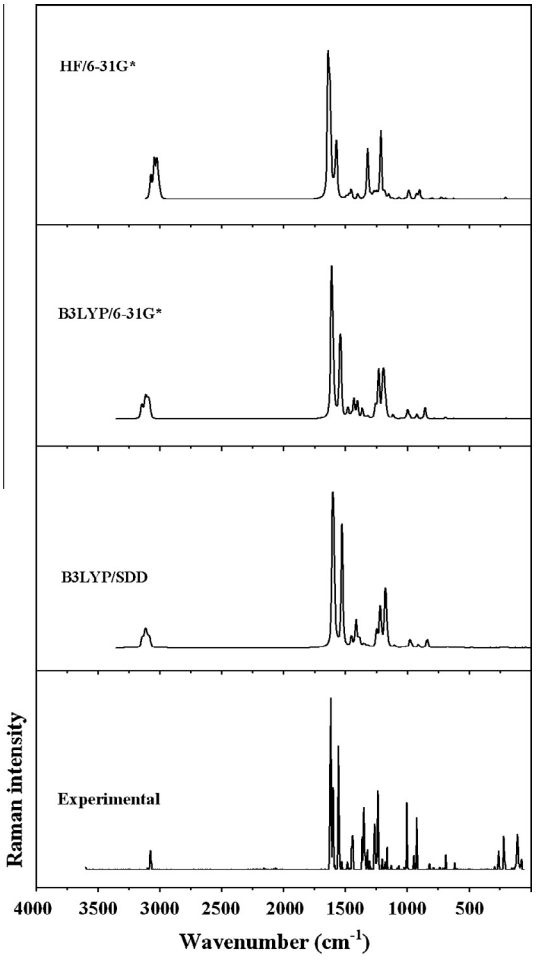

Fig. 2. FT-Raman spectrum of 5-nitro-2-phenylbenzoxazole.

known systematic errors due to the negligence of electron correlation [21]. We therefore, have used the scaling factor value of 0.8929 for HF/6-31G* basis set. The DFT hybrid B3LYP functional and SDD methods tend to overestimate the fundamental modes; therefore scaling factor of 0.9613 has to be used for obtaining a considerably better agreement with experimental data [21]. The Stuttagart/Dresden effective core potential basis set (SDD) [22] was chosen particularly because of its advantage of doing faster calculations with relatively better accuracy and structures [23]. Then wavenumber calculations were employed to confirm the structure as minimum points in energy. Parameters corresponding to optimized geometry (SDD) of the title compound (Fig. 3) are

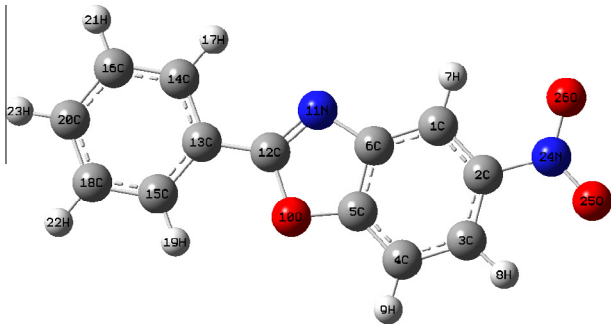

Fig. 3. Optimized geometry (B3LYP/SDD) of 5-nitro-2-phenylbenzoxazole.

Table 1
Optimized geometrical parameters (SDD) of 5-nitro-2-phenylbenzoxazole, atom labeling according to Fig. 3.

Bond lengths (Å)		Bond angles (°)		Dihedral angles (°)	
C_1—C_2	1.4061	C_2—C_1—C_6	115.9	C_2—C_1—C_6—N_{11}	180.0
C_1—C_6	1.3990	C_2—C_1—H_7	121.3	C_6—C_1—C_2—N_{24}	180.0
C_1—H_7	1.0828	C_6—C_1—H_7	122.7	H_7—C_1—C_2—C_3	180.0
C_2—C_3	1.4170	C_1—C_2—C_3	123.7	H_7—C_1—C_6—C_5	180.0
C_2—N_{24}	1.4780	C_1—C_2—N_{24}	118.2	C_1—C_2—C_3—H_8	180.0
C_3—C_4	1.4040	C_3—C_2—N_{24}	118.0	H_{22}—C_{18}—C_{20}—C_{16}	180.0
C_3—H_8	1.0836	C_2—C_3—C_4	120.1	C_{15}—C_{18}—C_{20}—H_{23}	180.0
C_4—C_5	1.3950	C_2—C_3—H_8	118.8	H_{21}—C_{16}—C_{20}—C_{18}	180.0
C_4—H_9	1.0839	C_4—C_3—H_8	121.1	C_{14}—C_{16}—C_{20}—H_{23}	180.0
C_5—C_6	1.4198	C_3—C_4—C_5	116.2	N_{24}—C_2—C_3—C_4	180.0
C_5—O_{10}	1.3948	C_3—C_4—H_9	121.7	C_1—C_2—N_{24}—O_{25}	180.0
C_6—N_{11}	1.4123	C_5—C_4—H_9	122.1	C_3—C_2—N_{24}—O_{26}	180.0
O_{10}—C_{12}	1.4360	C_4—C_5—C_6	123.8	C_2—C_3—C_4—H_9	180.0
N_{11}—C_{12}	1.3175	C_4—C_5—O_{10}	128.7	H_8—C_3—C_4—C_5	180.0
C_{12}—C_{13}	1.4571	C_6—C_5—O_{10}	107.5	H_{19}—C_{15}—C_{18}—C_{20}	180.0
C_{13}—C_{14}	1.4160	C_1—C_6—C_5	120.3	C_3—C_4—C_5—O_{10}	180.0
C_{13}—C_{15}	1.4148	C_1—C_6—N_{11}	130.8	H_9—C_4—C_5—C_6	180.0
C_{14}—C_{16}	1.4024	C_5—C_6—N_{11}	108.9	C_4—C_5—C_6—N_{11}	180.0
C_{14}—H_{17}	1.0860	C_5—O_{10}—C_{12}	104. 5	O_{10}—C_5—C_6—C_1	180.0
C_{15}—C_{18}	1.4042	C_6—N_{11}—C_{12}	106.0	C_4—C_5—O_{10}—C_{12}	180.0
C_{15}—H_{19}	1.0856	O_{10}—C_{12}—N_{11}	113.1	C_1—C_6—N_{11}—C_{12}	180.0
C_{16}—C_{20}	1.4107	O_{10}—C_{12}—C_{13}	117.5	C_5—O_{10}—C_{12}—C_{13}	180.0
C_{16}—H_{21}	1.0867	N_{11}—C_{12}—C_{13}	129.4	C_6—N_{11}—C_{12}—C_{13}	180.0
C_{18}—C_{20}	1.4093	C_{12}—C_{13}—C_{14}	119.0	O_{10}—C_{12}—C_{13}—C_{14}	180.0
C_{18}—H_{22}	1.0868	C_{12}—C_{13}—C_{15}	121.0	C_{13}—C_{15}—C_{18}—H_{22}	180.0
C_{20}—H_{23}	1.0872	C_{14}—C_{13}—C_{15}	120.0	H_{17}—C_{14}—C_{16}—C_{20}	180.0
N_{24}—O_{25}	1.2798	C_{13}—C_{14}—C_{16}	119.8	C_{13}—C_{14}—C_{16}—H_{21}	180.0
N_{24}—O_{26}	1.2791	C_{13}—C_{14}—H_{17}	119.0	C_{14}—C_{13}—C_{15}—H_{19}	180.0
		C_{16}—C_{14}—H_{17}	121.1	C_{12}—C_{13}—C_{15}—C_{18}	180.0
		C_{13}—C_{15}—C_{18}	119.7	C_{15}—C_{13}—C_{14}—H_{17}	180.0
		C_{13}—C_{15}—H_{19}	119.6	N_{11}—C_{12}—C_{13}—C_{15}	180.0
		C_{14}—C_{16}—C_{20}	120.2	C_{12}—C_{13}—C_{14}—C_{16}	180.0
		C_{18}—C_{15}—H_{19}	120.6		
		C_{14}—C_{16}—H_{21}	119.8		
		C_{20}—C_{16}—H_{21}	120.0		
		C_{15}—C_{18}—C_{20}	120.2		
		C_{15}—C_{18}—H_{22}	119.8		
		C_{20}—C_{18}—H_{22}	120.0		
		C_{16}—C_{20}—C_{18}	120.0		
		C_{16}—C_{20}—H_{23}	120.0		
		C_{18}—C_{20}—H_{23}	120.0		
		C_2—N_{24}—O_{25}	118.2		
		O_{25}—N_{24}—O_{26}	123.6		
		C_2—N_{24}—O_{26}	118.1		

given in Table 1. The absence of imaginary wavenumbers on the calculated vibrational spectrum confirms that the structure deduced corresponds to minimum energy. In total there are 72 vibrations (SDD) from 3146 to 42 cm^{-1}. The assignments of the calculated wavenumbers are aided by the animation option of GAUSSVIEW program, which gives a visual presentation of the vibrational modes [24]. The first hyperpolarizability (β_0) of this novel molecular system is calculated using SDD method, based on the finite field approach. In the presence of an applied electric field, the energy of a system is a function of the electric field. The natural bond orbital (NBO) calculations were performed using NBO3.1 program [25] as implemented in the Gaussian09 package at the DFT/B3LYP level in order to understand various second-order interactions between the filled orbital of one subsystem and vacant orbital of another subsystem. The potential energy distribution (PED) is calculated with the help of GAR2PED software package [26]. The ^{1}H NMR data were obtained from the DFT method using basis set 6-31G*. The characterization of excited states and electronic transitions were performed using the time-dependent DFT method (TD-B3LYP) on their correspondingly optimized ground state geometries. We used the time-dependent density functional theory (TD-DFT), which is found to be an accurate method for evaluating the low-lying excited states of molecules and has been thoroughly applied to

solve physical and chemical problems. Potential energy surface scan studies have been carried out to understand the stability of planar and non-planar structures of the molecule. The HOMO and LUMO energy were calculated by B3LYP/SDD method.

4. Results and discussion

4.1. Optimized geometry

A detailed potential energy surface (PES) scan on dihedral angles N_{11}—C_{12}—C_{13}—C_{14} and N_{11}—C_{12}—C_{13}—C_{15} have been performed at B3LYP/6-31G(d) level to reveal the possible conformations of 5-nitro-2-phenylbenzoxazole. The PES scan was carried out by minimizing the potential energy in all geometrical parameters by changing the torsion angle at every 10° for a 180° rotation around the bond. The results obtained in PES scan study by varying the torsion angle are plotted in Figs. 4 and 5. For the N_{11}—C_{12}—C_{13}—C_{14} the minimum energy was obtained at −0.0° in the potential energy curve of energy −835.14521 Hartrees. For the N_{11}—C_{12}—C_{13}—C_{15} the minimum energy occurs at 180.0° in the potential energy curve of energy −835.2174 Hartrees.

To best of our knowledge, the XRD crystal structure data of the title compound is not yet reported. In the following discussion, the phenyl rings attached with tri and mono substitution are assigned as PhI and PhII, respectively and the benzoxazole ring as RingIII. From the Table 1, the C—C bond length of C_5—C_6 (1.4198 Å) is greater than that of C_4—C_5 (1.395 Å) and C_1—C_6 (1.399 Å), because of the delocalization of electron density of C_5—C_6 with the ring III. Also C_5—O_{10}, C_{12}—O_{10}, C_6—N_{11} and C_{12}—N_{11} bond lengths are different because of the difference in their environment, also assumes a double bond character in C_{12}—N_{11}. The bond angle between C_{13}—C_{12}—O_{10} (117.5°) and C_{13}—C_{12}—N_{11} (129.4°) indicates the π bond character of the former. Bond angles of C_4—C_5—O_{10} (128.7) and C_1—C_6—N_{11} (130.8) are higher than 120° indicates the presence of hyper conjugative interaction. The broadening of C_5—C_4—H_9 (122.1) and C_6—C_1—H_7 (122.7) bond angles than that of other C—C—H bond angles also indicates the delocalization of charge in the III ring. The reduced bond angles of C_3—C_2—N_{24} (118.0), C_1—C_2—N_{24} (118.2) and H_8—C_3—C_2 (118.8) indicating the higher electronegative property of nitro group. The substitution of nitro group in the phenyl ring increases the C—C bond lengths C_1—C_2 and C_2—C_3 of the benzene ring. Nitro group is highly electronegative and tries to obtain additional electron density of the benzene ring. It attempts to draw it from the neighboring atoms, which move closer together,

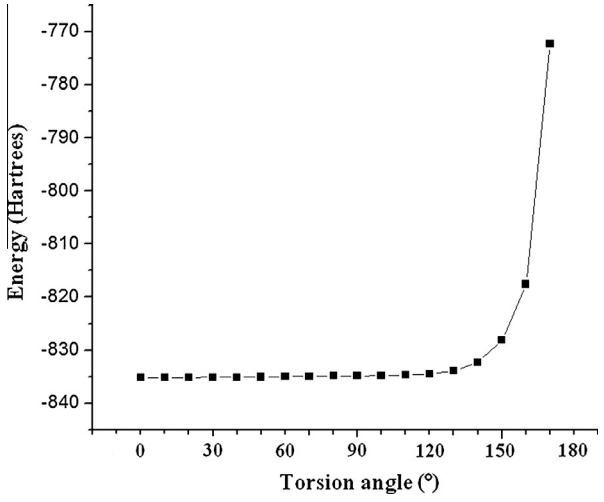

Fig. 4. Profile of potential energy scan for the torsion angle N11—C12—C13—C14.

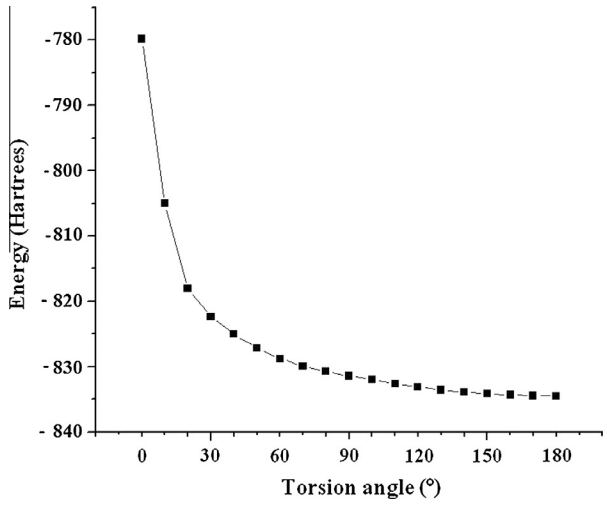

Fig. 5. Profile of potential energy scan for the torsion angle N11—C12—C13—C15.

in order to share the remaining electrons more easily. Due to this the bond angle A(1,2,3) is found to be 123.7° in the present calculation, which is 120° for normal benzene. Similarly, the bond lengths C_1—C_2 and C_2—C_3 are 1.4061 Å and 1.417 Å, respectively, which is 1.3864 Å for benzene. For the title compound the bond lengths C_5—O_{10}, C_6—N_{11} are found to be 1.3948 and 1.4123 Å while for 2-mercaptobenzoxazole [27] these are, respectively, 1.3436 and 1.3739 and for 5-nitro-2-(4-nitrobenzyl)benzoxazole, it is 1.398 and 1.42 Å respectively [28]. The bond lengths N_{11}—C_{12}, O_{10}—C_{12}, C_5—C_6 are found to increase to 1.3175, 1.436 and 1.4198 Å from the values 1.3001, 1.3804 and 1.3927 Å obtained for 2-mercaptobenzoxazole [29]. For 5-nitro-2-(4-nitrobenzyl) benzoxazole it is 1.3097, 1.4297 and 1.4183 Å respectively [28]. These changes in bond lengths for the title compound can be attributed to the conjugation of the phenyl ring in the neighboring position.

The aromatic ring of the title compound is somewhat irregular and the spread of CC bond distance is 1.395–1.4198 Å in PhI and 1.4024–1.416 Å in PhII, which is similar to the spread reported by Smith et al. [30]. For 5-nitro-2-(4-nitrobenzyl)benzoxazole the spread of CC bond distance is 1.3954–1.4183 Å and is very close to the title compound [28]. CH bond lengths in rings I and II of the title compound lie respectively between 1.0828–1.0839 Å and 1.0856–1.0872 Å. Chambers et al. [31] reported the N—O bond lengths in the range 1.2201–1.2441 Å and C—N bond length as 1.4544 Å. The experimental values of N—O bond lengths are 1.222–1.226 Å and C—N lengths in the range 1.442–1.460 Å [32]. Sundaraganesan et al. [33] reported C—N bond lengths as 1.453, 1.460 Å and N—O bond lengths in the range 1.2728–1.2748 Å. For the title compound, the C_2—N_{24} bond length is 1.4780 Å and N—O bond lengths are 1.2798, 1.2791 Å, which are in agreement with the reported values. The C_2—N_{24}—$O_{25,26}$ angles are reported [33] in the range 117.4–118.7°, where as for the title compound it is 118.1, 118.1°. Purkayastha and Chattopadhyay [34] reported N_{11}=C_{12}, N_{11}—C_6 bond lengths as 1.3270, 1.400 Å for benzothiazole and 1.3503, 1.407 Å for benzimidazole compounds. Ambujakshan et al. [18] has reported the same as 1.2753 and 1.3892 Å. In the present case, the corresponding bond lengths are 1.3175 and 1.4123 Å. Lifshitz et al. [35] reported the bond lengths for N_{11}—C_{12}, O_{10}—C_{12}, O_{10}—C_5, C_1—C_6, C_4—C_5, C_5—C_6, and N_{11}—C_6 as 1.291, 1.372, 1.374, 1.39, 1.4, 1.403 and 1.401 Å. The corresponding values in the present case are 1.3175, 1.436, 1.3948, 1.399, 1.395, 1.4198 and 1.4123 Å. Corresponding values are reported as 1.2753, 1.3492, 1.359, 1.3768, 1.3879, 1.3784, 1.3892 Å [18] and 1.2727, 1.347, 1.3594, 1.3884, 1.3777, 1.3776, 1.3903 Å [17]. The bond lengths C_4—O_{10}, C_3—N_{11}, N_{11}—C_{12}, C_{12}—O_{10} and C_3—C_4 are

found to be 1.3436, 1.3739, 1.3001, 1.3804 and 1.3827 Å for mercaptobenzoxazole [27]. The bond angles of the NO_2 group of the title compound O_{25}—N_{24}—O_{26}=123.6, O_{26}—N_{24}—C_2=118.1, and O_{25}—N_{24}—C_2=118.2° are in agreement with the values 123.5, 118.7, and 117.9° given by Saeed et al. [36].

4.2. IR and Raman spectra

The observed IR and Raman bands and calculated wavenumbers (scaled) and assignments are given in Table 2. The most characteristic bands in the spectra of nitro compounds are due to the NO_2 stretching vibrations. In nitro compounds, the asymmetric and symmetric NO_2 stretching vibrations are located in the regions 1661–1499 and 1389–1259 cm^{-1}, respectively [37,38]. Nitrobenzene derivatives display $\upsilon_{as}NO_2$ in the region 1535 ± 30 cm^{-1} and 3-nitropyridines at 1530 ± cm^{-1} [37,39] and in substituted nitro benzenes [37,38], υ_sNO_2 appears strongly at 1345 ± 30 cm^{-1}, in 3-nitropyridine at 1350 ± 20 cm^{-1} and in conjugated nitro alkenes [37] at 1345 ± 15 cm^{-1}. For the title compound, SDD calculations give NO_2 stretching vibrations at 1528 and 1351 cm^{-1} with bands at 1526, 1347 cm^{-1} in IR spectrum and at 1529, 1351 cm^{-1} in the Raman spectrum. The NO_2 scissors [37] occur at higher wavenumbers (850 ± 60 cm^{-1}) when conjugated to C—C or aromatic molecules, according to some investigators [40,41] with a contribution of the υCN which is expected near 1120 cm^{-1}. For the title compound, the SDD calculations give 758 cm^{-1} as δNO_2 mode. The scissoring NO_2 mode is reported at 759 cm^{-1} for a similar benzoxazole derivative [28]. In aromatic compounds the wagging mode ωNO_2 is assigned at 740 ± 50 cm^{-1} with a moderate to strong intensity, a region in which γCH also is active [37]. ωNO_2 is reported at 701 and 728 cm^{-1} for 1,2-dinitrobenzene and at 710 and 772 cm^{-1} for 1,4-dinitrobenzene [37] and 699, 663 cm^{-1} for 5-nitro-2 -(4-nitrobenzyl) benzoxazole [28]. For the title compound, the band at 702 cm^{-1} in IR and 709 cm^{-1} in the Raman spectrum is assigned as ωNO_2 mode. The SDD calculation gives 706 cm^{-1} as ωNO_2 mode. The rocking mode ρNO_2 is active in the region 540 ± 70 cm^{-1} in aromatic nitro compounds [37], Varsanyi et al. [42] found the region 70 ± 20 cm^{-1} and Suryanarayana et al. [43], 65 ± 10 cm^{-1} as the torsion of NO_2 for aromatic compounds. The rocking mode of NO_2 is reported at 522 cm^{-1} by the authors for 5-nitro-2-(4-nitrobenzyl)benzoxazole [28]. In the present case, the rocking mode of NO_2 is assigned at 479 cm^{-1} by the SDD calculations and 442 cm^{-1} in IR region.

The C=N stretching bands are observed in the range 1672–1566 cm^{-1} [17,38,44,45]. Saxena et al. [44] reported a value 1608 cm^{-1} for poly benzodithiazole and Klots and Collier [46] reported a value 1517 cm^{-1} for benzoxazole as υC=N stretching mode. The bands observed at 1526 cm^{-1} in IR and 1529 in Raman spectra and 1528 cm^{-1} given by calculation is assigned as υC=N for the title compound. The C=N stretching mode is reported at 1536 cm^{-1} for 5-nitro-2-(4-nitrobenzyl)benzoxazole [28]. The C—N stretching vibrations are observed in the region at 1330–1260 cm^{-1} due to stretching of the phenyl carbon–nitrogen bond [47]. For 2-mercaptobenzoxazole this mode [27] is reported at 1340 cm^{-1} (Raman) and 1325 cm^{-1} (ab initio calculations). Sandhyarani et al. [29] reported υCN at 1318 cm^{-1} for 2-mercaptobenzothiazole. For 5-nitro-2-(4-nitrobenzyl)benzoxazole, C—N stretching vibrations are observed in the region at 1228–1195 cm^{-1} [28]. In the present case, the SDD calculations give 1181, 1218 and at 1199 in IR and at 1201 cm^{-1} in Raman as C—N stretching modes.

As expected the asymmetric C—O—C vibration produce strong band at 1159 cm^{-1} in the IR, 1163 cm^{-1} in the Raman spectrum with SDD value at 1162 cm^{-1}. The symmetric C—O—C stretching vibration is observed at 1066 cm^{-1} in the IR spectrum, 1078 cm^{-1} in the Raman spectrum and at 1070 cm^{-1} theoretically as expected [37,38]. The C—O—C stretching is reported at 1250 and 1073 cm^{-1} for 2-mercaptobenzoxazole [38,27] and 1153 and 1073 cm^{-1} for 5-nitro-2-(4-nitrobenzyl)benzoxazole [28].

The existence of one or more aromatic rings in the structure is normally readily determined from the C—H and C=C—C ring related vibrations. The C—H stretching occurs above 3000 cm^{-1} and is typically exhibited as a multiplicity of weak to moderate bands, compared with the aliphatic C—H stretch [48]. Klot and Collier [46] reported the bands at 3085, 3074, 3065 and 3045 cm^{-1} as υCH modes for benzoxazole. For 5-nitro-2-(4-nitrobenzyl)benzoxazole the bands are observed in the range 3087–3146 cm^{-1}[28]. The bands observed at 3099, 3069 cm^{-1} in the IR and 3075 cm^{-1} in the Raman spectrum are assigned as the C—H stretching modes of the phenyl rings. The SDD calculations give these modes in the range 3077–3146 cm^{-1}.

The benzene ring possesses six ring stretching vibrations, of which the four with the highest wavenumbers (occurring near 1600, 1580, 1490 and 1440 cm^{-1}) are good group vibrations. In the absence of ring conjugation, the band near 1580 cm^{-1} is usually weaker than that at 1600 cm^{-1}. The fifth ring stretching vibration which is active near 1335 ± 35 cm^{-1} a region which overlaps strongly with that of the CH in-plane deformation and the intensity is in general, low or medium high [37]. The sixth ring stretching vibration or ring breathing mode appears as a weak band near 1000 cm^{-1} in mono, 1,3-di and 1,3,5-trisubstituted benzenes. In the otherwise substituted benzene, however, this vibration is substituent sensitive and difficult to distinguish from the ring in-plane deformation. Since the identification of all the normal modes of vibrations of large molecules is not trivial, we tried to simplify the problem by considering each molecule as substituted benzene. Such an idea has already been successfully utilized by several workers for the vibrational assignments of molecules containing multiple homo- and hetero aromatic rings [28,49–51]. The modes in the two phenyl rings will differ in wavenumber and the magnitude of splitting will depend on the strength of interactions between different parts (internal coordinates) of the two rings. For some modes, this splitting is so small that they may be considered as quasi-degenerate and for the other modes a significant amount of splitting is observed. Such observations have already been reported [28,49–51].

For the title compound, the bands observed at 1446 cm^{-1} in the IR and 1600, 1585, 1441, 1365 cm^{-1} in the Raman spectrum are assigned as υPhI modes with 1593, 1582, 1436, 1415, 1389 cm^{-1} as SDD values. In asymmetric tri-substituted benzene, when all the three substituents are light, the ring breathing mode falls in the range 500–600 cm^{-1}; when all the three substituents are heavy, it appears in the range 1050–1100 cm^{-1} and in the case of mixed substituents, it falls in the range 600–750 cm^{-1} [52]. Madhavan et al. [53] reported the ring breathing mode for a compound having two tri-substituted benzene rings as 1110 cm^{-1} and 1083 cm^{-1}. For the title compound, PED analysis gives the ring breathing mode at 1043 cm^{-1} (SDD) with 1044 cm^{-1} in IR and 1067 cm^{-1} in Raman which is in agreement with the literature [28,54]. For tri-substituted benzenes δCH modes are expected in the range 1050–1280 cm^{-1} [37]. For the phenyl ring PhI, the bands observed at 1263, 1237, 1125 cm^{-1} in the IR spectrum and at 1263, 1237, 1129 cm^{-1} in the Raman spectrum are assigned as in-plane CH deformation modes. Also SDD calculations give these modes at 1247, 1246, 1102 cm^{-1} which are in agreement with literature [37,28].

For mono substituted benzene, the υPh modes are expected in the range of 1285–1610 cm^{-1} [37]. For the title compound, the υPhII modes are assigned at 1603, 1564, 1453, 1424, 1331 cm^{-1} theoretically and bands are observed at 1616, 1551, 1481, 1320 cm^{-1} in IR spectrum and at 1618, 1556, 1483, 1322 cm^{-1} in Raman spectrum. The ring breathing mode for mono substituted

Table 2
Calculated (Scaled) wavenumbers, IR, Raman bands and assignments of 5-nitro-2-phenylbenzoxazole.

HF/6-31G*			B3LYP/6-31G*			B3LYP/SDD			IR	Raman	Assignments
υ	IR_I	R_A	υ	IR_I	R_A	υ	IR_I	R_A	υ	υ	–
3079	11.73	47.96	3153	8.01	49.60	3146	9.38	54.56	–	–	υCHI(96)
3073	5.28	95.84	3144	4.29	108.66	3140	2.96	94.81	–	–	υCHI(96)
3055	2.25	55.95	3125	2.45	66.43	3121	2.47	47.79	–	–	υCHI(99)
3044	5.85	166.55	3117	7.41	176.25	3119	15.89	227.37	–	–	υCHII(99)
3040	7.15	32.32	3113	7.37	16.80	3111	11.88	15.33	–	–	υCHII(93)
3026	27.88	154.01	3099	27.35	206.38	3101	21.96	131.96	–	–	υCHII(100)
3016	13.57	120.43	3089	12.75	139.73	3088	11.28	108.97	3099	–	υCHII(99)
3003	0.03	49.78	3077	0.05	47.35	3077	0.09	31.69	3069	3075	υCHII(95)
1639	179.70	1032.44	1613	86.37	1482.47	1603	84.72	1537.11	1616	1618	υPhI(24), υPhII(58)
1623	9.79	454.91	1602	0.35	719.38	1593	1.06	1034.32	–	1600	υPhI(66), υPhII(20)
1612	9.96	55.77	1594	4.97	19.19	1582	6.13	8.09	–	1585	υPhI(66), υPhII(21)
1594	13.99	66.86	1573	0.53	31.75	1564	0.69	32.36	1551	1556	υPhII(63)
1575	135.96	417.79	1542	82.80	1237.75	1528	96.97	1456.04	1526	1529	υN_{11}—C_{12} (50), υNO_2(45)
1493	63.61	17.69	1482	61.55	114.21	1453	72.10	132.50	1481	1483	υN_{11}—C_{12} (11), υPhII(50)
1473	108.19	18.78	1457	44.78	17.65	1436	36.50	16.73	1446	1441	υPhI(54), δCHI(17)
1455	74.87	10.56	1451	7.17	28.35	1424	6.33	6.82	–	–	δCHII(49), υPhII(49)
1453	102.54	49.45	1431	77.96	196.12	1415	85.81	336.85	–	–	υPh I(66), υCN(16)
1399	173.38	34.38	1404	49.46	169.97	1389	50.77	153.75	–	1365	υNO_2(19), υPhI(67)
1344	3.85	9.93	1365	26.84	95.27	1351	51.52	61.99	1347	1351	υPhI(25) υNO_2(62)
1321	329.64	275.46	1339	7.87	25.38	1331	2.41	18.71	1320	1322	υPhII(76), δCHII(13)
1297	27.78	21.89	1319	1.56	28.36	1312	3.25	22.48	–	1306	δCHII(57), υPhII (27)
1272	55.38	49.52	1259	29.31	66.58	1247	78.24	235.40	1263	1263	δCHI(48), υCC(10)
1253	26.99	40.19	1257	37.93	59.01	1246	3.16	19.19	1237	1237	δCHI(50), υCO(10), υPhI(16)
1237	14.89	17.81	1233	382.04	567.93	1218	356.50	601.45	–	1201	υNO_2(49), υCN(47)
1215	82.61	357.94	1198	24.34	478.30	1181	31.67	479.44	1199	–	υNC(45), υPhI(17)
1186	4.97	17.85	1188	40.77	336.03	1173	43.89	371.44	–	1178	δCHII(59), υCN(19)
1183	24.06	33.17	1179	0.13	13.24	1162	8.80	19.88	1159	1163	δCHII(56), υCO(23)
1149	3.25	28.15	1172	21.53	81.74	1162	10.99	52.24	1159	1163	υCO(47), δCHII(37)
1119	18.55	7.07	1116	28.05	37.51	1102	27.92	29.36	1125	1129	δCHI (45) υCO(11), υPhI(25)
1079	2.72	1.90	1085	4.76	0.90	1070	7.14	0.54	1066	1078	υCO(43), δCHII(47)
1067	0.11	3.45	1051	17.61	8.01	1043	23.19	6.17	1044	1067	δCHI(21), υPhI(50)
1066	11.89	7.32	1027	0.78	3.40	1012	1.61	10.74	1022	1025	υPhII(66), δCHII(18)
1043	0.01	0.04	1005	0.25	2.07	1012	0.26	1.37	–	1004	δCHII(81), τPhII(11)
1033	0.12	0.05	998	21.99	99.79	996	0.02	0.14	1001	–	γCHII(91)
1031	29.69	1.69	981	63.69	24.23	980	0.49	0.71	–	–	γCHI(87)
1016	44.23	4.69	979	0.01	0.05	978	18.28	113.02	–	–	δPhII(72), γCHI(11)
996	4.67	3.11	970	0.87	0.38	963	72.21	25.32	–	–	δRingII(29), γCHII(18), γCHI(27)
988	15.16	66.65	941	3.69	2.79	950	5.05	0.05	945	947	γCHII(84)
985	31.72	0.28	925	4.28	49.23	936	30.17	0.28	920	923	γCHI(77), τPhI(10)
925	6.03	40.39	923	25.32	0.79	909	47.65	5.10	891	–	δPhI(11), γCHI(18), γCHII(52)
902	9.15	48.82	858	28.39	126.79	861	0.05	0.01	860	–	γCHII(100)

(*continued on next page*)

Table 2 (*continued*)

HF/6-31G*			B3LYP/6-31G*			B3LYP/SDD			IR	Raman	Assignments
υ	IR_I	R_A	υ	IR_I	R_A	υ	IR_I	R_A	υ	υ	–
891	0.01	2.52	853	0.01	4.58	840	138.88	29.49	–	–	δRingII(32), δPhI(24), δPhII(18)
874	50.46	1.66	831	30.73	2.85	839	40.49	0.17	837	820	γCHI(80), τPhI(10)
819	8.52	1.62	808	39.68	1.49	798	34.73	0.77	820	–	δPhII(34), δPhI(28)
807	27.41	2.96	782	25.60	0.49	784	42.61	2.33	777	787	τPhII(24), γCH II(50), γCC(15)
797	79.13	6.42	779	48.47	6.47	758	7.68	47.04	–	–	δNO_2(46), δPhI(14)
759	4.39	0.48	726	1.52	0.43	752	0.53	0.22	737	736	τPhI(60), τRingIII(27)
727	100.7	14.45	698	59.89	8.76	706	3.19	64.19	702	709	γNO_2(41), γCN(22), τRingIII(13)
712	44.29	2.97	693	25.89	1.53	695	47.60	0.14	–	689	τPhII(51), γCHII(29), γCC(12)
702	4.51	0.03	691	2.69	10.29	680	0.61	0.23	686	–	τPhII(27), τRingIII(25), γCC(23)
691	2.09	3.86	679	0.19	0.28	675	2.77	12.31	–	–	δPhII(46), δRingIII(15), δPhI(10)
685	38.21	4.02	675	25.47	2.62	659	27.39	2.92	–	–	δRingII(33), δNO_2 (24), δPhI(22)
625	0.34	6.49	625	0.55	6.52	609	0.56	9.36	618	617	δPhII(87)
588	1.01	2.22	586	0.29	2.99	576	0.57	2.62	595	–	δPhI(34), δPhII(12), δRingIII(10)
581	0.02	0.93	567	0.02	1.49	563	0.06	1.18	–	–	τPhI(52), γCN(19), γNO_2(10)
555	2.31	0.61	553	0.85	0.79	543	0.91	1.19	556	–	δPh I(39), δNO_2 (19), δCC(14)
502	4.54	0.08	491	2.48	0.10	488	7.06	0.03	489	–	τPhII(38), γCC(25), τRingIII(18)
491	6.50	0.96	490	3.22	3.32	479	3.23	3.82	442	–	δNO_2 (44), δCC(21), δCN(11)
438	3.39	0.03	426	2.31	0.05	429	3.28	0.01	423	–	τPhI(59), τRingIII(21) τPhII(16)
416	0.01	0.08	406	0.01	0.07	402	0.01	0.03	–	–	τPhII(84)
391	2.97	0.63	388	1.06	0.38	381	1.17	0.46	–	–	δPhI(25), δPhII(24), γCC(11)
353	0.06	0.11	342	0.02	0.08	343	0.07	0.10	–	–	τPhII(23), τRingIII(22), τPhI(15), γCN(14)
334	3.46	0.48	332	3.07	0.37	326	3.01	0.43	–	–	δCC(27), δPhI(20), δNO_2 (14), δCN(11)
288	2.28	0.85	281	1.49	0.89	279	1.17	0.81	–	262	γCN(15), τRingIII(20), τPhI(11), τPhII(19)
247	0.31	4.32	247	0.07	3.72	243	0.06	4.36	–	–	δPhII(15), δPhI(26), δRingIII(18)
206	2.18	8.49	201	1.30	7.66	200	1.19	5.57	–	220	τPhII(26), τPhI(19), τRingIII(30)
197	3.65	1.78	194	1.96	1.99	190	2.15	2.08	–	–	δCN(50), δCC(15)
126	4.17	1.28	123	2.73	1.33	123	2.95	0.75	–	109	γCN(16), γCC(23),

Table 2 (*continued*)

HF/6-31G*			B3LYP/6-31G*			B3LYP/SDD			IR	Raman	Assignments
υ	IR_I	R_A	υ	IR_I	R_A	υ	IR_I	R_A	υ	υ	–
											τRingIII(25)
81	0.54	0.29	82	0.43	0.38	79	0.44	0.36	–	–	δCC(76)
59	0.84	1.11	68	0.84	0.81	67	0.99	0.75	–	–	τCN(63), τCC(20)
43	0.07	0.93	46	0.13	0.17	46	0.09	0.03	–	–	τCN(36), τCC(35)
40	0.37	1.47	43	0.16	2.23	42	0.16	1.67	–	–	τCC(37), γCC(23), τRingIII(12)

υ-Stretching; δ-in-plane deformation; γ-out-of-plane deformation; τ-torsion; PhI-tri-substituted phenyl ring; PhII-mono substituted phenyl ring; RingIII-benzoxazole ring; potential energy distribution is given in brackets with the assignments in the last column; IR_I-IR intensity; R_A-Raman activity.

benzenes appears near 1000 cm^{-1} [37]. For the title compound, this is confirmed by the band at 1022 cm^{-1} in the IR spectrum, 1025 cm^{-1} in the Raman spectrum which finds support from the computational results 1012 cm^{-1}. For mono substituted benzene, the in-plane CH vibrations are expected in the range of 1015–1300 cm^{-1} [37]. Bands observed at 1159, 1066 cm^{-1} in the IR spectrum and at 1306, 1178, 1163, 1078, 1004 cm^{-1} in the Raman spectrum are assigned as δCH modes for the ring PhII. The corresponding theoretical values (SDD) are 1312, 1173, 1162, 1070 and 1012 cm^{-1}.

The C—H out-of-plane deformations γCH are observed between 1000 and 700 cm^{-1} [37]. γCH vibrations are mainly determined by the number of adjacent hydrogen atoms on the ring. Although strongly electron attracting substituent groups, such as nitro-, can result in an increase (about 30 cm^{-1}) in the wavenumber of the vibration, these vibrations are not very much affected by the nature of the substituent. Generally the C—H out-of-plane deformations with the highest wavenumbers have a weaker intensity than those absorbing at lower wavenumbers. Most of the deformation bands of the CH vibrations of the phenyl rings are not pure but contain significant contributions for other modes (Table 2). The out-of-plane γCH modes are observed at 920, 837 cm^{-1} in the IR spectrum, 923, 820 cm^{-1} in the Raman spectrum for PhI and at 1001, 945, 891, 860, 777 cm^{-1} in the IR spectrum and at 947, 787 cm^{-1} in Raman spectrum for PhII. The corresponding SDD values are 980, 936, 839 cm^{-1} for PhI and 996, 950, 909, 861,784 cm^{-1} for PhII.

The benzoxazole ring stretching vibrations exist in the range 1504–1309 cm^{-1} in both spectra [44,55]. According to literature, bands observed at 1504, 1433, 1418 cm^{-1} in the Raman spectrum and 1499, 1474, 1412 and 1309 cm^{-1} in the IR spectrum are assigned as the ring stretching vibrations [44]. Klots and Collier [46] reported the bands at 1615, 1604, 1475 and 1451 cm^{-1} as fundamental ring vibrations of the benzoxazole ring. For benzoxazole, Klots and Collier [46] reported the bands at 932, 847 and 746 cm^{-1} as out-of-plane deformations for the benzene ring. According to Collier and Klots [56] the non-planar vibrations are observed at 970, 932, 864, 847, 764, 620, 574, 417, 254, 218 cm^{-1} for benzoxazole and at 973, 939, 856, 757, 729, 584, 489, 419, 207, 192 cm^{-1} for benzothiazole. The planar modes below 1000 cm^{-1} for benzoxazole are reported to be at 920, 870, 778, 622, 538, 413 cm^{-1} and for benzothiazole at 873, 801, 712, 666, 531, 504, 530 cm^{-1} [56]. We have also observed the planar and non-planar modes for the title compound in this region. The substitutent sensitive modes of the rings and deformation modes are also identified and assigned (Table 2).

In order to investigate the performance of vibrational wavenumbers of the title compound, the root mean square (RMS) value between the calculated and observed wavenumbers were calculated. The RMS values of wavenumbers were calculated using the following expression:

$$\mathrm{RMS} = \sqrt{\frac{1}{n-1}\sum_{i}^{n}(\upsilon_i^{calc} - \upsilon_i^{exp})^2}.$$

The RMS error of the observed IR and Raman bands are found to 33.16, 30.10 for HF/6-31G*, 14.47, 14.34 for B3LYP/6-31G* and 13.52, 13.39 for B3LYP/SDD methods, respectively. The small differences between experimental and calculated vibrational modes are observed. This is due to the fact that experimental results belong to solid phase and theoretical calculations belong to gaseous phase.

4.3. First hyperpolarizability

Nonlinear optics deals with the interaction of applied electromagnetic fields in various materials to generate new electromagnetic fields, altered in wavenumber, phase, or other physical properties [57]. Organic molecules able to manipulate photonic signals efficiently are of importance in technologies such as optical communication, optical computing, and dynamic image processing [58,59]. In this context, the static first hyperpolarizability of the title compound is also calculated in the present study. The first hyperpolarizability (β_0) of this novel molecular system is calculated using SDD basis set, based on the finite field approach. The calculated first hyperpolarizability of the title compound is 101.0×10^{-30} esu, which is comparable with the reported values of similar derivatives [60] and which is 776.92 times that of the standard NLO material urea (0.13×10^{-30} esu) [61]. We conclude that the title compound is an attractive object for future studies of nonlinear optical properties.

4.4. NBO analysis

NBO analysis provides the most accurate possible 'natural Lewis structure' picture of NBO acceptor orbital 'j' because all orbital details are mathematically chosen to include the highest possible percentage of the electron density. A useful aspect of the NBO method is that it gives information about interactions of both filled and virtual orbital spaces that could enhance the analysis of intra and inter molecular interactions. The second-order Fock-matrix was carried out to evaluate the donor-acceptor interactions in the NBO basis. The interactions result in a loss of occupancy from the localized NBO of the idealized Lewis structure into an empty non-Lewis orbital. For each donor (i) and acceptor (j) the stabilization energy (E2) associated with the delocalization i → j is determined as

$$E(2) = \Delta E_{ij} = q_i \frac{(F_{i,j})^2}{(E_j - E_i)}$$

where $q_i \rightarrow$ donor orbital occupancy, E_i, $E_j \rightarrow$ orbital energies, $F_{i,j} \rightarrow$ the off diagonal NBO Fock matrix element.

In NBO analysis large E(2) value shows the intensive interaction between electron-donors and electron-acceptors and greater the extent of conjugation of the whole system, the possible intensive interactions are given in Table 3. The second-order perturbation theory analysis of Fock matrix in NBO basis shows strong intra-molecular hyper conjugative interactions of π electrons. The intra-molecular hyper conjugative interactions are formed by the orbital overlap between n(O) and π^*(N—O) bond and n(O) and π^*(C—N) bond orbital which results in ICT causing stabilization of the system. The strong intra-molecular hyper conjugative interaction of N_{24}—O_{26} from O_{25} of n3(O_{25}) $\rightarrow \pi^*$(N_{24}—O_{26}) which increases ED (0.66e) that weakens the respective bonds leading to stabilization of 166.97 kcal mol^{-1}. Also there is another hyper conjugative interaction observed in n2(O_{10}) $\rightarrow \pi^*$(N_{11}—C_{12}) bond, having ED (0.30e) with a stabilization of 27.63 kcal mol^{-1}. These interactions are observed as an increase in electron density (ED) in N—O and N—C anti-bonding orbitals that weakens the respective bonds. The increased electron density at the oxygen atoms leads to the elongation of respective bond length and a lowering of the corresponding stretching wavenumber. The electron density (ED) is transferred from the n(O) to the anti-bonding π^* orbital of the N—O and N—C bonds, explaining both the elongation and the red shift [62]. The C=N and NO_2 stretching modes can be used as a good probe for evaluating the bonding configuration around the N atoms and the electronic distribution of the benzene molecule. Hence the 5-nitro-2-phenylbenzoxazole structure is stabilized by these orbital interactions. The NBO analysis also describes the bonding in terms of the natural hybrid orbital n2(O_{26}), which occupy a higher energy orbital (−0.30608 a.u.) with considerable p-character (99.82%) and low occupation number (1.91210 a.u.) and the other n1(O_{26}) occupy a lower energy orbital (−0.82723) with p-character (19.57%) and high occupation number (1.97745 a.u). Thus, a very close to pure p-type lone pair orbital participates in the electron donation to the σ^*(N—O) orbital for n2(O_{26}) $\rightarrow \sigma^*$(C—C) interaction in the compound. The results are tabulated in Table 4.

4.5. Mulliken charges and molecular electrostatic potential

The calculation of atomic charges plays an important role in the application of quantum mechanical calculations to molecular systems. Mulliken charges are calculated by determining the electron population of each atom as defined in the basis functions. The charge distributions calculated by Mulliken [63] and NBO methods for the equilibrium geometry of 5-nitro-2-phenylbenzoxazole are given in Table 5. The charge distribution on the molecule has an important influence on the vibrational spectra. In 5-nitro-2-phenylbenzoxazole the Mulliken atomic charge of the carbon atoms in the neighborhood of C_2, C_5, C_{13} become more positive, shows the direction of delocalization and shows that the natural atomic charges are more sensitive to the changes in the molecular structure than Mulliken's net charges. (The results are represented in Fig. S1 as Supporting material). Also we have done a comparison of Mulliken charges obtained by different basis sets and tabulated

Table 3
Second-order perturbation theory analysis of Fock matrix in NBO basis corresponding to the intra molecular bonds of the title compound.

Donor (i)	Type	ED/e	Acceptor (i)	Type	ED/e	E(2)[a]	E(j) − E(i)[b]	F(i,j)[c]
C1—C2	σ	1.97	C2—C3	σ*	0.02	2.93	1.21	0.053
–	–	–	C3—H8	–	0.01	2.3	1.23	0.048
–	–	–	C6—N11	–	0.02	6.34	1.11	0.075
–	–	–	N24—O25	–	0.06	3.01	1.02	0.05
C1—C6	σ	1.97	C2—N24	σ*	0.10	5.23	0.97	0.07
–	–	–	C5—C6	–	0.05	2.18	1.19	0.05
–	–	–	C5—O10	–	0.03	2.06	0.99	0.04
–	–	–	N11—C12	–	0.02	2.15	1.21	0.05
C1—C6	π	1.60	C2—C3	π*	0.42	20.75	0.28	0.07
–	–	–	C4—C5	–	0.39	24.09	0.28	0.07
–	–	–	N11—C12	–	0.30	13.91	0.26	0.05
C1—H7	σ	1.97	C2—C3	σ*	0.02	5.74	1.03	0.07
–	–	–	C5—C6	–	0.05	5.30	1.00	0.07
C2—C3	σ	1.98	C1—C2	σ*	0.02	2.95	1.22	0.05
–	–	–	C1—H7	–	0.01	2.57	1.22	0.05
–	–	–	C4—H9	–	0.01	2.95	1.21	0.05
–	–	–	N24—O26	–	0.06	2.95	1.02	0.05
C2—C3	π	1.63	C1—C6	π*	0.37	22.87	0.29	0.07
–	–	–	C4—C5	–	0.39	18.16	0.28	0.06
–	–	–	N24—O26	–	0.66	36.15	0.12	0.06
C2—N24	σ	1.99	C1—C6	σ*	0.02	2.21	1.34	0.05
–	–	–	C3—C4	–	0.01	2.22	1.34	0.05
C3—C4	σ	1.97	C2—N24	σ*	0.10	4.63	0.96	0.06
–	–	–	C5—O10	–	0.03	7.30	0.97	0.08
C3—H8	σ	1.97	C1—C2	σ*	0.02	5.96	1.04	0.07
–	–	–	C4—C5	–	0.02	4.61	1.05	0.06
C4—C5	σ	1.98	C3—H8	σ*	0.01	3.07	1.25	0.06
–	–	–	C5—C6	–	0.05	2.54	1.21	0.05
–	–	–	O10—C12	–	0.08	2.51	0.95	0.04
C4—C5	π	1.63	C1—C6	π*	0.37	18.56	0.30	0.07
–	–	1.63	C2—C3	–	0.42	23.70	0.29	0.07
C4—H9	σ	1.98	C2—C3	σ*	0.02	4.95	1.03	0.06
–	–	–	C5—C6	–	0.05	5.34	1.01	0.07
C5—C6	σ	1.98	C1—C6	σ*	0.02	2.68	1.24	0.05
–	–	–	C1—H7	–	0.01	3.16	1.21	0.06
–	–	–	C4—C5	–	0.02	3.10	1.23	0.06
–	–	–	C4—H9	–	0.01	3.10	1.20	0.06
C5—O10	σ	1.99	C1—C6	σ*	0.02	3.18	1.43	0.06

Table 3 (*continued*)

Donor (i)	Type	ED/e	Acceptor (i)	Type	ED/e	E(2)[a]	E(j) − E(i)[b]	F(i,j)[c]
–	–	–	C12—C13	–	0.03	3.05	1.35	0.06
C6—N11	σ	1.97	C4—C5	σ*	0.02	3.77	1.29	0.06
–	–	–	C12—C13	–	0.03	7.51	1.23	0.09
O10—C12	σ	1.98	C4—C5	σ*	0.02	4.80	1.37	0.07
–	–	–	C13—C14	–	0.02	2.55	1.38	0.05
N11—C12	σ	1.98	C1—C6	σ*	0.02	5.41	1.41	0.08
–	–	–	C12—C13	–	0.03	2.23	1.33	0.05
–	–	–	C13—C15	–	0.02	2.31	1.40	0.05
N11—C12	π	1.86	C1—C6	π*	0.37	18.43	0.35	0.08
–	–	–	C13—C15	–	0.39	9.35	0.36	0.06
C12—C13	σ	1.97	C5—O10	σ*	0.03	2.47	0.96	0.04
–	–	–	C6—N11	–	0.02	3.59	1.09	0.06
–	–	–	N11—C12	–	0.02	2.00	1.19	0.04
–	–	–	C14—C16	–	0.01	2.89	1.25	0.54
–	–	–	C15—C18	–	0.01	2.73	1.24	0.05
C13—C14	σ	1.97	O10—C12	σ*	0.08	4.25	0.89	0.06
–	–	–	C12—C13	–	0.03	2.02	1.14	0.04
–	–	–	C13—C15	π*	0.02	2.97	1.21	0.05
–	–	–	C15—H19	–	0.01	2.83	1.20	0.05
–	–	–	C16—H21	–	0.01	2.95	1.20	0.05
C13—H15	σ	1.97	N11—C12	σ*	0.02	3.81	1.18	0.06
–	–	–	C13—C14	π*	0.02	2.95	1.21	0.05
–	–	–	C14—H17	–	0.01	2.66	1.21	0.05
–	–	–	C18—H22	–	0.01	2.90	1.20	0.05
C13—C15	π	1.63	N11—C12	π*	0.30	27.79	0.24	0.07
–	–	–	C14—C16	–	0.29	20.17	0.29	0.07
–	–	–	C18—C20	–	0.32	19.44	0.28	0.07
C14—C16	σ	1.98	C12—C13	σ*	0.03	4.42	1.14	0.06
–	–	–	C20—H23	–	0.01	2.93	1.21	0.05
C14—C16	π	1.65	C13—C15	π*	0.39	20.58	0.28	0.07
–	–	–	C18—C20	–	0.32	22.11	0.28	0.07
C14—H17	σ	1.98	C13—C15	σ*	0.02	5.64	1.03	0.07
–	–	–	C16—C20	–	0.02	4.85	1.05	0.06
C15—C18	σ	1.98	C12—C13	σ*	0.03	4.73	1.14	0.07
–	–	–	C15—H19	–	0.01	0.79	1.20	0.03
-	–	–	C20—H23	–	0.01	2.93	1.21	0.05
C15—H19	σ	1.98	C13—C14	σ*	0.02	5.61	1.04	0.07
–	–	–	C18—C20	–	0.02	4.81	1.05	0.06
C16—C20	σ	1.98	C14—H17	σ*	0.01	3.08	1.21	0.05
–	–	–	C18—H22	–	0.01	3.05	1.20	0.05
C16—H21	σ	1.98	C13—C14	σ*	0.02	5.25	1.04	0.07
–	–	–	C18—C20	–	0.02	4.84	1.05	0.06
C18—C20	σ	1.98	C15—H19	σ*	0.01	3.06	1.20	0.05
–	–	–	C16—H21	–	0.01	3.02	1.20	0.05
C18—C20	π	1.64	C13—C15	π*	0.39	23.31	0.28	0.07
–	–	–	C14—C16	–	0.29	19.18	0.28	0.07
C18—H22	σ	1.98	C13—C15	σ*	0.02	5.26	1.04	0.07
–	–	–	C16—C20	–	0.02	4.85	1.05	0.06
C20—H23	σ	1.98	C14—C16	σ*	0.01	4.87	1.07	0.06
–	–	–	C15—C18	–	0.01	4.93	1.06	0.07
N24—O26	π	1.98	C2—C3	π*	0.42	4.73	0.44	0.05
–	–	–	N24—O26	–	0.66	8.58	0.27	0.05
LP (1)O10	n	1.97	C5—C6	σ*	0.05	3.94	1.07	0.06
–	–	–	N11—C12	–	0.02	3.85	1.10	0.06
LP (2)O10	n	1.75	C4—C5	σ*	0.39	26.27	0.35	0.09
–	–	–	N11—C12	π*	0.30	27.63	0.33	0.09
LP (1)N11	n	1.91	C5—C6	σ*	0.05	7.08	0.84	0.07
–	–	–	O10—C12	–	0.08	15.45	0.58	0.08
LP (1)O25	n	1.98	C2—N24	σ*	0.10	5.39	1.06	0.07
–	–	–	N24—O26	–	0.06	2.20	1.11	0.05
LP (2)O25	n	1.91	C1—C2	σ*	0.02	0.74	0.79	0.02
–	–	–	C2—N24	–	0.10	10.39	0.54	0.07
–	–	–	N24—O26	–	0.06	18.01	0.59	0.09
LP (3)O25	n	1.44	N24—O26	π*	0.66	166.97	0.11	0.12
LP(1)O26	n	1.98	C2—N24	σ*	0.10	5.40	1.06	0.07
–	–	–	N24—O25	–	0.06	2.22	1.11	0.05
LP(2)O26	n	1.91	C2—N24	σ*	0.10	10.46	0.54	0.07
–	–	–	N24—O25	–	0.06	18.10	0.59	0.09

[a] E(2) means energy of hyperconjugative interactions (stabilization energy).
[b] Energy difference between donor and acceptor i and j NBO orbitals.
[c] F(i, j) is the Fock matrix element between i and j NBO orbitals.

Table 4
NBO results showing the formation of Lewis and non-Lewis orbitals.

Bond (A–B)	ED/energy[a]	EDA%	EDB%	NBO	s%	p%
σC1—C2	1.97206	49.44	50.56	0.7031($sp^{1.92}$)C	34.19	65.81
–	−0.73947	–	–	+0.7111($sp^{1.63}$)C	37.95	62.05
σC1—C6	1.97197	49.41	50.59	0.7029($sp^{1.85}$)C	35.10	64.90
–	−0.74074	–	–	+0.7112($sp^{1.58}$)C	38.69	61.31
πC1—C6	1.60353	45.91	54.09	0.6776($sp^{1.00}$)C	0.00	100.0
–	−0.29166	–	–	+0.7354($sp^{1.00}$)C	0.00	100.0
σC2—C3	1.97563	50.96	49.04	0.7139($sp^{1.64}$)C	37.86	62.14
–	−0.73600	–	–	+0.7003($sp^{1.92}$)C	34.30	65.70
πC2—C3	1.62716	55.28	44.72	0.7435($sp^{1.00}$)C	0.00	100.0
–	−0.29485	–	–	0.6688($sp^{1.00}$)C	0.00	100.0
σC2—N24	1.98654	36.62	63.38	0.6052($sp^{3.15}$)C	24.07	75.93
–	−0.83235	–	–	+0.7961($sp^{1.69}$)N	37.16	62.84
σC3—C4	1.96949	49.79	50.21	0.7057($sp^{1.80}$)C	35.72	64.28
–	−0.72799	–	–	+0.7086($sp^{1.82}$)C	35.41	64.59
σC4—C5	1.97688	49.20	50.80	0.7014($sp^{1.93}$)C	34.10	65.90
–	−0.75408	–	–	+0.7127($sp^{1.45}$)C	40.85	59.15
πC4—C5	1.62701	50.52	49.48	0.7107($sp^{1.00}$)C	0.00	100.0
–	−0.30212	–	–	+0.7034($sp^{1.00}$)C	0.00	100.0
σC5—C6	1.97537	50.20	49.80	0.7085($sp^{1.86}$)C	34.96	65.04
–	−0.73095	–	49.80	+0.7057($sp^{2.11}$)C	32.17	67.83
σC5—O10	1.98539	31.05	68.95	0.5572($sp^{3.16}$)C	24.05	75.95
–	−0.91760	–	–	+0.8304($sp^{2.35}$)O	29.89	70.11
σC6—N11	1.96927	40.91	59.09	0.6396($sp^{1.79}$)C	28.98	71.02
–	−0.79138	–	–	+0.7687($sp^{1.80}$)N	30.58	69.42
σO10—C12	1.98386	70.35	29.65	0.8387($sp^{2.68}$)O	27.18	72.82
–	−0.87194	–	–	+0.5445($sp^{3.22}$)C	23.69	76.31
σN11—C12	1.98085	59.79	40.21	0.7732($sp^{1.84}$)N	35.26	64.74
–	−0.89469	–	–	+0.6341($sp^{1.84}$)C	35.16	64.84
πN11—C12	1.86395	59.53	40.47	0.7716($sp^{1.00}$)C	0.00	100.0
–	−0.35148	–	–	+0.6361($sp^{1.00}$)C	0.00	100.0
σC12—C13	1.96880	50.02	49.98	0.7073($sp^{1.43}$)C	41.16	58.84
–	−0.71750	–	–	+0.7070($sp^{2.26}$)C	30.71	69.29
σC13—C14	1.96930	51.57	48.43	0.7181($sp^{1.90}$)C	34.48	65.52
–	−0.70260	–	–	+0.6959($sp^{1.89}$)C	34.63	65.37
σC13—C15	1.97328	51.46	48.54	0.7174($sp^{1.87}$)C	34.80	65.20
–	−0.70708	–	–	+0.6967($sp^{1.87}$)C	34.82	65.18
πC13—C15	1.62702	53.68	46.32	0.7327($sp^{1.00}$)C	0.00	100.0
–	−0.27003	–	–	+0.6806($sp^{1.00}$)C	0.00	100.0
σC14—C16	1.97909	50.29	49.71	0.7092($sp^{1.81}$)C	35.63	64.37
–	−0.70772	–	–	+0.7051($sp^{1.81}$)C	35.53	64.47
πC14—C16	1.65366	48.57	51.43	0.6969($sp^{1.00}$)C	0.00	100.0
–	−0.26693	–	–	+0.7171($sp^{1.00}$)C	0.00	100.0
σC15—C18	1.97911	50.38	49.62	0.7098($sp^{1.81}$)C	35.63	64.37
–	−0.70779	–	–	+0.7044($sp^{1.82}$)C	35.48	64.52
σC16—C20	1.98153	50.00	50.00	0.7071($sp^{1.84}$)C	35.23	64.77
–	−0.70365	–	–	+0.7071($sp^{1.83}$)C	35.35	64.65
σC18—C20	1.98156	50.04	49.96	0.7074($sp^{1.83}$)C	35.30	64.70
–	−0.70488	–	–	+0.7068($sp^{1.83}$)C	35.38	64.62
πC18—C20	1.63981	51.94	49.06	0.7137($sp^{1.00}$)C	0.00	100.0
–	−0.26621	–	–	+0.7004($sp^{1.00}$)C	0.00	100.0
σN24—O25	1.99141	49.42	50.58	0.7030($sp^{2.20}$)N	31.26	68.74
–	−1.02893	–	–	+0.7112($sp^{4.15}$)O	19.43	80.57
σN24—O26	1.99140	49.42	50.58	0.7030($sp^{2.20}$)N	31.29	68.71
–	−1.02969	–	–	+0.7112($sp^{4.14}$)O	19.45	80.55
πN24—O26	1.98398	41.40	58.60	0.6434($sp^{1.00}$)C	0.00	100.0
–	−0.45184	–	–	+0.7655($sp^{1.00}$)C	0.00	100.0
n1O10	1.97285	–	–	$sp^{1.33}$	42.93	57.07
–	−0.62082	–	–	–	–	–
n2O10	1.74652	–	–	$sp^{1.00}$	0.00	100.0
–	−0.36662	–	–	–	–	–
n1N11	1.90602	–	–	$sp^{1.93}$	34.18	65.82
–	−0.38441	–	–	–	–	–
n1O25	1.97758	–	–	$sp^{0.24}$	80.44	19.56
–	−0.82761	–	–	–	–	–
n2O25	1.91244	–	–	$sp^{99.99}$	0.19	99.81
–	−0.30645	–	–	–	–	–
n3O25	1.43958	–	–	$sp^{1.00}$	0.00	100.0
–	−0.28848	–	–	–	–	–
n1O26	1.97745	–	–	$sp^{0.24}$	80.43	19.57
–	−0.82723	–	–	–	–	–
n2O26	1.91210	–	–	$sp^{99.99}$	0.18	99.82
–	−0.30608	–	–	–	–	–

[a] ED/energy is expressed in a.u.

Table 5
The charge distribution calculated (SDD) by the Mulliken and natural bond orbital (NBO) methods.

Atom	Mulliken charge	Natural Charge
1C	−0.472279	−0.17929
2C	0.390931	0.07032
3C	−0.329578	−0.18800
4C	−0.305583	−0.23718
5C	0.249229	0.31596
6C	0.076886	0.10944
7H	0.308151	0.27044
8H	0.288512	0.26100
9H	0.260587	0.24551
10O	−0.298106	−0.52244
11N	−0.058384	−0.50856
12C	0.090886	0.58891
13C	0.314634	−0.13302
14C	−0.352504	−0.16444
15C	−0.337259	−0.17762
16C	−0.212801	−0.20853
17H	0.267916	0.24201
18C	−0.214293	−0.20864
19H	0.258406	0.23657
20C	−0.215870	−0.19202
21H	0.229448	0.22603
22H	0.227457	0.22513
23H	0.229144	0.22429
24N	0.064746	0.44528
25O	−0.233407	−0.37212
26O	−0.226866	−0.36906

Table 6
Calculated Mulliken charges of 5-nitro-2-phenylbenzoxazole by HF6/31G*, B3LYP/6-31G* and B3LYP/SDD basis sets.

Atom	HF/6-31G*	B3LYP/6-31G*	B3LYP/SDD
1C	−0.012314	−0.061956	−0.472238
2C	0.183470	0.290654	0.390167
3C	−0.149467	−0.138176	−0.330318
4C	−0.149857	−0.111134	−0.305618
5C	0.384843	0.309622	0.249631
6C	0.031129	0.084601	0.077228
7H	0.312716	0.207330	0.308269
8H	0.285729	0.190803	0.288746
9H	0.258470	0.170705	0.260672
10O	−0.773336	−0.548172	−0.298048
11N	−0.529712	−0.394853	−0.058831
12C	0.571447	0.317045	0.091808
13C	−0.085198	0.073982	0.314875
14C	−0.138577	−0.111985	−0.352364
15C	−0.146893	−0.119630	−0.337202
16C	−0.220293	−0.141442	−0.212622
17H	0.261472	0.174560	0.267854
18C	−0.219359	−0.140761	−0.214347
19H	0.253400	0.164764	0.258327
20C	−0.171920	−0.104252	−0.216106
21H	0.214114	0.140129	0.229291
22H	0.212401	0.138385	0.227361
23H	0.213477	0.138780	0.229099
24N	0.221927	0.051765	0.064443
25O	−0.407528	−0.293600	−0.233327
26O	−0.400140	−0.287164	−0.226747

it in Table 6 in order to assess the sensitivity of the calculated charges to changes in (i) the choice of the basis set; (ii) the choice of the quantum mechanical method. (The results can, however, better be represented in graphical form as shown in Fig. S2 as Supporting material). We have observed a change in the charge distribution by changing different basis sets.

MEP is related to the ED and is a very useful descriptor in understanding sites for electrophilic and nucleophilic reactions as well as hydrogen bonding interactions [64,65]. The electrostatic potential V(r) is also well suited for analyzing processes based on

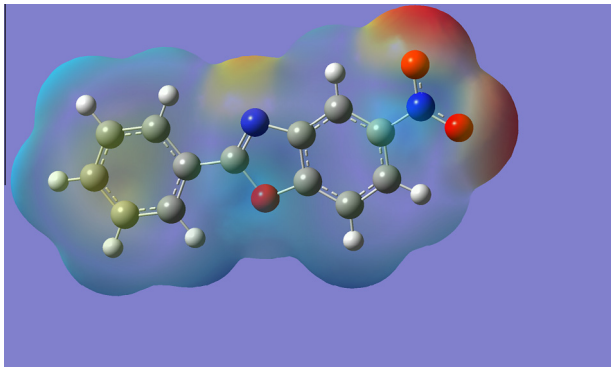

Fig. 6. Molecular electrostatic potential map calculated at B3LYP/SDD level.

Table 7
Calculated electronic absorption spectrum of 5-nitro-2-phenylbenzoxazole using TD-DFT/B3LYP/SDD.

Excitation	CI expansion Coefficient	Energy (eV)	Wavelength calc. (nm)	Wavelength Exp. (nm)	Oscillator Strength (f)
Excited state 1					
60 → 64	0.10525	3.5451	349.73	301	0.0647
62 → 63	0.67049	–	–	–	–
Excited State 2					
60 → 63	−0.19352	3.9733	312.04	267	0.2436
61 → 63	−0.26264	–	–	–	–
62 → 64	0.53508	–	–	–	–
Excited State 3					
60 → 63	0.27240	4.0225	308.22	232	0.6037
61 → 63	0.47298	–	–	–	–
62 → 64	0.30857	–	–	–	–
Excited State 4					
60 → 63	0.54440	4.3020	288.20	212	0.0814
61 → 63	−0.37662	–	–	–	–
61 → 64	0.10606	–	–	–	–

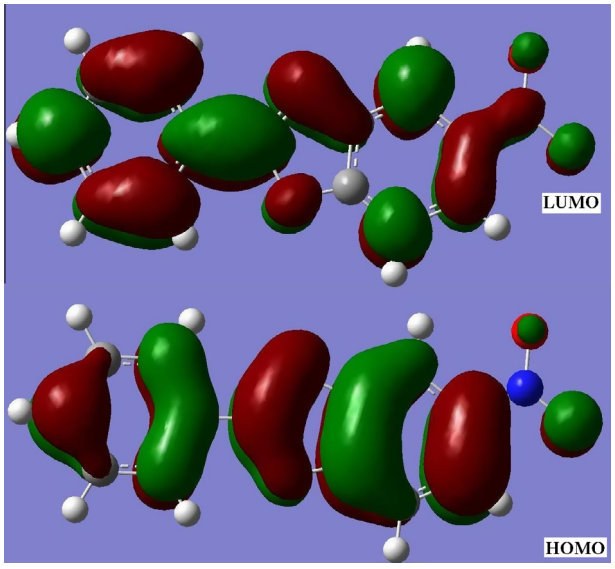

Fig. 7. HOMO–LUMO plot of 5-nitro-2-phenylbenzoxazole.

the "recognition" of one molecule by another, as in drug-receptor, and enzyme-substrate interactions, because it is through their potentials that the two species first "see" each other [64,66]. To

Table 8
Experimental and calculated ^{1}H NMR parameters (with respect to TMS).

Proton	σ_{TMS}	B3LYP/6-31G σ_{calc}	$\delta_{calc(\sigma\ TMS-\sigma calc)}$	Exp δ_{ppm}
H7	32.7711	23.8419	8.9292	8.654
H8	–	24.0088	8.7623	8.341
H9	–	24.8233	7.9478	8.648
H19	–	24.1801	8.591	8.313
H21	–	24.9001	7.871	7.550
H22	–	24.9005	7.8706	7.619
H23	–	24.8398	7.9313	7.700

Table 9
Antimicrobial activity results (MIC lg/ml) of title compound with the standard drugs Micro- organisms.

–	Microorganisms						Fungus
–	Gram-positive			Gram-negative			–
–	S.a.	S.f.	B.s.	E.c.	K.p.	P.A.	C.a.
Title compound	25	50	25	25	25	50	25
Ampicillin	1.56	1.56	1.56	12.5	25	>200	–
Amoxycillin	1.56	1.56	1.56	3.12	12.5	>200	–
Tetracycline	1.56	1.56	1.56	3.12	3.12	50	–
Streptomycin	3.12	100	50	1.56	1.56	100	–
Clotrimazol	–	–	–	–	–	–	6.25
Haloprogin	–	–	–	–	–	–	3.12

Abbreviations: *E.c., Escherichia coli; K.p., Klepsiella pneumoniae; P.a., Pseudomonas aeruginosa; S.a., Staphylococcus aureus; S.f., Streptococcus faecalis; B.s., Bacillus subtilis; C.a., Candida albicans.*

predict reactive sites of electrophilic and nucleophilic attacks for the investigated molecule, MEP at the B3LYP/6-31G(d,p) optimized geometry was calculated. The negative (red and yellow) regions of MEP were related to electrophilic reactivity and the positive (blue) regions to nucleophilic reactivity (Fig. 6). From the MEP it is evident that the negative charge covers the NO_2 group, nitrogen atom of the benzoxazole group and the positive region is over the phenyl rings. The more electro negativity in the nitro group makes it the most reactive part in the molecule.

4.6. Electronic absorption spectra

Electronic transitions are usually classified according to the orbitals engaged or to specific parts of the molecule involved. Common types of electronic transitions in organic compounds are π–π^*, n–π^* and π^*(acceptor)–π(donor).The UV–visible bands in 5-nitro-2-phenylbenzoxazole are observed at 301, 267, 232 and 212 nm. Observed band at 212 nm is due to the π–π^*. The less intense band centered at 267 nm is due to the partly forbidden n–π^* transition from HOMO to LUMO. The more intense band observed at 301 nm belonged to the dipole-allowed π–π^* transition. In order to understand the electronic transitions of 5-nitro-2-phenylbenzoxazole, TD-DFT calculation on electronic absorption spectrum in vacuum was performed. TD-DFT calculation is capable of describing the spectral features of 5-nitro-2-phenylbenzoxazole because of the qualitative agreement of line shape and relative strength as compared with experiment. The absorption spectra of organic compounds stem from the ground-to-excited state vibrational transition of electrons. The intense band in the UV range of the electronic absorption spectrum is observed at 301 nm, which is indicating the presence of chromophoric NO_2 in the ring. The calculated three lowest-energy transitions of the molecule from TD-DFT method and the observed electronic transitions are listed in Table 7. From the table, the calculated energy transitions are red shifted from the experimental value, because these bands are observed in gas phase without considering the solvent effect.

The conjugated molecules are characterized by a highest occupied molecular orbital–lowest unoccupied molecular orbital (HOMO–LUMO) separation, which is the result of a significant degree of ICT from the end-capping electron-donor groups to the efficient electron-acceptor groups through π-conjugated path. The strong charge transfer interaction through π-conjugated bridge results in substantial ground state donor–acceptor mixing and the appearance of a charge transfer band in the electronic absorption spectrum. Therefore, an ED transfer occurs from the more aromatic part of the π-conjugated system in the electron-donor side to its electron-withdrawing part. The atomic orbital components of the frontier molecular orbitals are shown in Fig. 7. The HOMO–LUMO energy gap value is found to be 3.209 eV, which is responsible for the bioactive property of the title compound. The HOMO–LUMO energy gap is reported as 0.132 eV for 5-nitro-2-(4-nitrobenzyl)benzoxazole [28], 4.3424 eV for 5-[(4-bromophenyl)acetamido]-2-(4-tert-butylphenyl)benzoxazole [67] and 3.592 eV for 2-(p-nitro benzyl)benzoxazole [68].

4.7. ^{1}H NMR spectrum

The experimental spectrum data of 5-nitro-2-phenylbenzoxazole in DMSO with TMS as internal standard is obtained at 400 MHz and is given in Table 8. The absolute isotropic chemical shielding of 5-nitro-2-phenylbenzoxazole was calculated by B3LYP/GIAO model [69]. Relative chemical shifts were then estimated by using the corresponding TMS shielding: σ_{calc}.(TMS). It could be seen from Table 8 that chemical shift was in agreement with the experimental ^{1}H NMR data. Thus, the results showed that the predicted proton chemical shifts were in good agreement with the experimental data for 5-nitro-2-phenylbenzoxazole.

4.8. Antimicrobial properties

Benzoxazoles are the structural isosteres of natural nucleotides and interact easily with the biopolymers that they constitute an important class of heterocyclic compounds with antimicrobial and antibiotic activity [5]. When a nitro group was attached at position 5 of the fusedheterocyclic system caused twofold better potency against *Escherichia coli*. On the other hand, the SAR results against *Candida albicans* revealed that the electron withdrawing groups such as chlorine or nitro attached at position 5 of the heterocyclic nucleus increased the potency. So that the minimum inhibitory concentrations (MIC) of the title compound against *Staphylococcus aureus, Streptococcus faecalis, Bacillus subtilis* as Gram-positive and *E. coli, Klebsiella Klebsiella pneumoniae, Pseudomonas aeruginosa* as Gramnegative bacteria and the yeast *C. albicans* by using twofold serial dilution technique and compared to ampicillin, amoxycillin, tetracycline, streptomycin, clotrimazole and haloprogin as standard drugs. All the biological results of the compounds were given in Table 9. The combined data reported that the compounds were able to inhibit the in vitro growth of screened microorganisms showing MIC values between 100 and 3.12 μg/ml.

5. Conclusion

The geometry optimization of the title compound has been carried out using DFT and SDD level. The simultaneous activation of the phenyl ring stretching modes in IR and Raman spectra are evidence for charge transfer interaction between the donor and the acceptor group through the π system. This is responsible for the bioactivity of the molecule. The NBO analysis confirms the ICT formed by the orbital overlap between n(O) and σ^*(N—O). A very close to pure p-type lone pair orbital participates in the electron donation to the $\sigma*$(C—C) orbital for n2(O_{26}) → σ^*(N—O). The TD-DFT calculations on the molecule provided deep insight into their electronic structures and properties. In addition, the calculated ^{1}H NMR and UV–Vis results are all in good agreement with the experimental data. The lowering of HOMO–LUMO band gap supports bioactive property of the molecule. MEP predicts the most reactive part in the molecule. The calculated first hyperpolarizability is comparable with the reported values of similar derivatives and is an attractive object for future studies of non linear optics. Microbiological results indicated that the title compound possessed a broad spectrum activity against the tested Gram-positive, Gram-negative bacteria.

Acknowledgements

The authors are thankful to University of Antwerp for access to the university's CalcUA Supercomputer Cluster. BJB thanks University Grants Commission, India, for a research fellowship.

Appendix A. Supplementary material

Supplementary data associated with this article can be found, in the online version, at http://dx.doi.org/10.1016/j.molstruc.2014.01.018.

References

[1] A.D. Rodriguez, C. Ramirez, I.L. Rodriguez, E. Gonzalez, Org. Lett. 1 (1999) 527.
[2] J. Kobayashi, T. Madono, H. Shigemori, Tetraahedron Lett. 36 (1995) 5589.
[3] M. Yamato, J. Pharm. Soc. Jpn. 112 (1992) 81.
[4] T. Hisano, M. Ichikawa, K. Tsumoto, M. Tasaki, Chem. Pharm. Bull. 30 (1982) 2996.
[5] M. Prudhomme, J. Guyot, G. Jeminet, J. Antibiot. 39 (1986) 934.
[6] S. Ersan, S. Nacak, R. Berkem, T. Ozden, Arzneium. Forsch. Drug Res. 47 (1997) 963.
[7] D.B. Olsen, S.S. Carroll, J.C. Culberson, J.A. Shafer, L.C. Kuo, Nucl. Acids Res. 22 (1996) 1437.
[8] S. Staszewski, F.E. Massari, A. Kober, R. Gohler, S. Durr, K.W. Anderson, C.L. Schneider, J.A. Waterbury, K.K. Bakshi, V.I. Taylor, C.S. Hildebrand, C. Kreisl, B. Hoffstedt, W.A. Schleif, H. von Breisen, H.R. Waigmann, G.B. Calandra, J.L. Ryan, W. Stille, E.A. Emini, V.W. Byrnes, J. Infect. Dis. 171 (1995) 1159.
[9] M.B. Reynolds, M.R. DeLuca, S.M. Kerwin, Bioorg. Chem. 27 (1999) 326.
[10] M. Ueki, K. Ueno, S. Miyadoh, K. Abe, K. Shibata, M. Taniguchi, S. Oi, J. Antibiot. 46 (1993) 1089.
[11] M.R. DeLuca, S.M. Kerwin, Tetrahedron Lett. 38 (1997) 199.
[12] K. Devinder, M.R. Jacob, M.B. Reynolds, S.m. Kerwin, Bioorg. Med. Chem. 10 (2002) 3997.
[13] I. Yalcin, E. Sener, S. Ozden, A. Akin, S. Yildiz, J. Pharm. Sci. 11 (1986) 257.
[14] E. Sener, S. Ozden, I. Yalcin, T. Ozden, A. Akin, S. Yildiz, J. Pharm. Sci. 11 (1986) 190.
[15] S. Ozden, T. Ozden, E. Sener, I. Yalcin, A. Akin, S. Yildiz, J. Pharm. Sci. 12 (1987) 39.
[16] E. Sener, I. Yalcin, S. Ozden, T. Ozden, A. Akin, S. Yildiz, J. Med. Pharm. 11 (1987) 391.
[17] P.L. Anto, C.Y. Panicker, H.T. Varghese, D. Philip, O. Temiz-Arpaci, B. Tekiner-Gulbas, I. Yildiz, Spectrochim. Acta Part A 67 (2007) 744.
[18] K.R. Ambujakshan, V.S. Madhavan, H.T. Varghese, C.Y. Panicker, O. Temiz-Arpaci, B. Tekiner-Gulbas, I. Yildiz, Spectrochim. Acta 69 (2008) 782.
[19] I. Yalcin, E. Sener, T. Ozden, S. Ozden, A. Akin, Eur. J. Med. Chem. 25 (1990) 705.
[20] Gaussian 09, Revision B.01, M.J. Frisch, G.W. Trucks, H.B. Schlegel, G.E. Scuseria, M.A. Robb, J.R. Cheeseman, G. Scalmani, V. Barone, B. Mennucci, G.A. Petersson, H. Nakatsuji, M. Caricato, X. Li, H.P. Hratchian, A.F. Izmaylov, J. Bloino, G. Zheng, J.L. Sonnenberg, M. Hada, M. Ehara, K. Toyota, R. Fukuda, J. Hasegawa, M. Ishida, T. Nakajima, Y. Honda, O. Kitao, H. Nakai, T. Vreven, J.A. Montgomery, Jr., J.E. Peralta, F. Ogliaro, M. Bearpark, J.J. Heyd, E. Brothers, K.N. Kudin, V.N. Staroverov, T. Keith, R. Kobayashi, J. Normand, K. Raghavachari, A. Rendell, J.C. Burant, S.S. Iyengar, J. Tomasi, M. Cossi, N. Rega, J.M. Millam, M. Klene, J.E. Knox, J.B. Cross, V. Bakken, C. Adamo, J. Jaramillo, R. Gomperts, R.E. Stratmann, O. Yazyev, A.J. Austin, R. Cammi, C. Pomelli, J.W. Ochterski, R.L. Martin, K. Morokuma, V.G. Zakrzewski, G.A. Voth, P. Salvador, J.J. Dannenberg, S. Dapprich, A.D. Daniels, O. Farkas, J.B. Foresman, J.V. Ortiz, J. Cioslowski, D.J. Fox, Gaussian Inc, Wallingford CT, 2010.
[21] J.B. Foresman, in: E. Frisch (Ed.), Exploring Chemistry with Electronic Structure Methods: A Guide to Using Gaussian, Gaussian Inc., Pittsburg, PA, 1996.
[22] P.J. Hay, W.R. Wadt, J. Chem. Phys. 82 (1985) 270.
[23] J.Y. Zhao, Y. Zhang, L.G. Zhu, J. Mol. Struct. Theochem. 671 (2004) 179.
[24] GaussView, Version 5, R. Dennington, T. Keith, J. Millam, Semichem Inc., Shawnee Mission KS, 2009.

[25] NBO Version 3.1, E.D. Glendening, A. E. Reed, J.E. Carpenter, F. Weinhold.
[26] J.M.L. Martin, C. Van Alsenoy, GAR2PED, A Program to Obtain a Potential Energy Distribution from a Gaussian Archive Record, University of Antwerp, Belgium, 2007.
[27] A. Bigotto, B. Pergolese, J. Raman Spectrosc. 32 (2001) 953.
[28] J.B. Bhagyasree, H.T. Varghese, C.Y. Panicker, J. Samuel, C. Van Alsenoy, K. Bolelli, I. Yildiz, E. Aki, Spectrochim. Acta 102 (2013) 99.
[29] N. Sandhyarani, G. Skanth, S. Berchmanns, V. Yegnaraman, T. Pradeep, J. Colloid Interface Sci. 209 (1999) 154.
[30] G. Smith, D.E. Lynch, K.A. Byriel, C.H.L. Kennard, Aust. J. Chem. 48 (1995) 1133.
[31] R.D. Chambers, M.A. Fox, G. Sandford, J. Trmcic, A. Goeta, J. Fluorine Chem. 128 (2007) 29.
[32] N. Okabe, T. Nakamura, H. Fukuda, Acta Cryst. C49 (1993) 1678.
[33] N. Sundaraganesan, S. Ayyappan, H. Umamaheswari, B.D. Joshua, Spectrochim. Acta 66A (2007) 17.
[34] P. Purkayastha, N. Chattopadhyay, Phys. Chem. Chem. Phys. 2 (2003) 203.
[35] A. Lifshitz, C. Tamburu, A. Suslensky, F. Dubnikova, J. Phys. Chem. A 110 (2006) 4607.
[36] A. Saeed, S. Hussain, U. Florke, Turk. J. Chem. 32 (2008) 481.
[37] N.P.G. Roeges, A Guide to the Complete Interpretation of Infrared Spectra of Organic Structures, Wiley, New York, 1994.
[38] R.M. Silverstein, F.X. Webster, Spectrometric Identification of Organic Compounds, sixth ed., John Wiley, Asia, 2003.
[39] A. Perjessy, D. Rasala, P. Tomasik, R. Gawinecki, Collect. Czech. Chem. Commun. 50 (1985) 2443.
[40] Y.S. Mary, H.T. Varghese, C.Y. Panicker, T. Ertan, I. Yildiz, O. Temiz-Arpaci, Spectrochim. Acta 71 (2008) 566.
[41] L. Ushakumari, H.T. Varghese, C.Y.T. Ertan, I. Yildiz, J. Raman Spectrosc. 39 (2008) 1832.
[42] G. Varsanyi, E. Molner-Pall, K. Kosa, G. Keresztury, Acta Chim. Acad. Sci. Hung. 106 (1979) 481.
[43] V. Suryanarayana, A.P. Kumar, G.R. Rao, G.C. Panday, Spectrochim. Acta 48A (1992) 1481.
[44] R. Saxena, L.D. Kaudpal, G.N. Mathur, J. Polym. Sci. Part A: Polym. Chem. 40 (2002) 3959.
[45] K. Nakamoto, Infrared and Raman Spectrum of Inorganic and coordination Compounds, 5th ed., John Wiley and Sons Inc, New York, 1997.
[46] T.D. Klots, W.B. Collier, Spectrochim. Acta 51A (1995) 1291.
[47] N.B. Colthup, L.H. Daly, S.E. Wiberly, Introduction to Infrared and Raman Spectroscopy, 3rd ed., Academic Press, Boston, 1990.
[48] J. Coates, in: R.A. Meyers (Ed.), Encyclopedia of Analytical Chemistry; Interpretation of Infrared Spectra, A Practical Approach, John Wiley and Sons Ltd., Chichester, 2000.
[49] M. Kaur, Y.S. Mary, H.T. Varghese, C.Y. Panicker, H.S. Yathirajan, M.S. Siddegowda, C. Van Alsenoy, Spectrochim. Acta 98 (2012) 91.
[50] V.S. Madhavan, Y.S. Mary, H.T. Varghese, C.Y. Panicker, S. Mathew, C. Van Alsenoy, J. Vinsova, Spectrochim. Acta 89 (2012) 308.
[51] A. Chandran, H.T. Varghese, Y.S. Mary, C.Y. Panicker, T.K. Manojkumar, C. Van Alsenoy, G. Rajendran, Spectrochim. Acta 87 (2012) 29.
[52] G. Varsanyi, Assignments of Vibrational Spectra of Seven Hundred Benzene Derivatives, Wiley, New York, 1974.
[53] V.S. Madhavan, H.T. Varghese, S. Mathew, J. Vinsova, C.Y. Panicker, Spectrochim. Acta 72A (2009) 547.
[54] C.Y. Panicker, H.T. Varghese, K.R. Ambujakshan, S. Mathew, S. Ganguli, A.K. Nanda, C. Van Alsenoy, Y.S. Mary, J. Mol. Struct. 963 (2010) 137.
[55] W. Kunyi, C.W. Park, M.S.K. kim, K. Kim, Bull. Korean Chem. Soc. 8 (1987) 291.
[56] W.B. Collier, T.D. Klots, Spectrochim. Acta 51A (1995) 1255.
[57] Y.R. Shen, The Principles of Nonlinear Optics, Wiley, New York, 1984.
[58] P.V. Kolinsky, Opt. Eng. 31 (1992) 1676.
[59] D.F. Eaton, Science 25 (1991) 281.
[60] L.N. Kuleshova, M.Y. Antipin, V.N. Khrustalev, D.V. Gusev, G.V. Grintselev-Knyazev, E.S. Bobrikova, Cryst. Reports 48 (2003) 594.
[61] M. Adant, M. Dupuis, J.L. Bredas, Int. J. Quantum. Chem. 56 (1995) 497.
[62] J. Choo, S. Kim, H. Joo, Y. Kwon, J. Mol. Struct. (Theochem.) 587 (2002) 1.
[63] R.S. Mulliken, J. Chem. Phys. 23 (1955) 1833.
[64] E. Scrocco, J. Tomasi, Adv. Quantum. Chem. 103 (1978) 115.
[65] F.J. Luque, J.M. Lopez, M. Orozco, Theor. Chem. Acc. 103 (2000) 343.
[66] P. Politzer, J.S. Murray, in: D.L. Beveridge, R. Lavery (Eds.), Theoretical Biochemistry and Molecular Biophysics: A Comprehensive Survey, vol. 2, Protein, Adenine Press, Schenectady, NY, 1991. Chap. 13.
[67] J.B. Bhagyasree, J. Samuel, H.T. Varghese, C.Y. Panicker, M. Arisoy, O. Temiz-Arpaci, Spectrochim. Acta 115 (2013) 79.
[68] J.B. Bhagyasree, H.T. Varghese, C.Y. Panicker, J. Samuel, C. Van Alsenoy, S. Yilmaz, I. Yildiz, E. Aki, J. Mol. Struct. 1046 (2013) 92.
[69] K. Wolinski, J.F. Hinton, P. Pulay, J. Am. Chem. Soc. 112 (1990) 8251.